View metadata, citation and similar papers at core.ac.uk

brought to you by CORE

provided by University of Groningen

University of Groningen

The Numerical Solution of the Navier-Stokes Equations for Laminar, Incompressible Flow past a Parabolic Cylinder

Botta, E.F.F.; Dijkstra, D.; Veldman, A.E.P.

Published in:
Default journal

IMPORTANT NOTE: You are advised to consult the publisher's version (publisher's PDF) if you wish to cite from it. Please check the document version below.

Document Version
Publisher's PDF, also known as Version of record

Publication date:
1972

Link to publication in University of Groningen/UMCG research database

Citation for published version (APA):
Botta, E. F. F., Dijkstra, D., & Veldman, A. E. P. (1972). The Numerical Solution of the Navier-Stokes Equations for Laminar, Incompressible Flow past a Parabolic Cylinder. Default journal.

Copyright
Other than for strictly personal use, it is not permitted to download or to forward/distribute the text or part of it without the consent of the author(s) and/or copyright holder(s), unless the work is under an open content license (like Creative Commons).

Take-down policy
If you believe that this document breaches copyright please contact us providing details, and we will remove access to the work immediately and investigate your claim.

Downloaded from the University of Groningen/UMCG research database (Pure): http://www.rug.nl/research/portal. For technical reasons the number of authors shown on this cover page is limited to 10 maximum.

Download date: 12-11-2019

Journal of Engineering Mathematics, Vol. 6, No. 1, January 1972
Wolters-Noordhoff Publishing–Groningen
Printed in the Netherlands

The Numerical Solution of the Navier–Stokes Equations for Laminar, Incompressible Flow past a Parabolic Cylinder

E. F. F. BOTTA, D. DIJKSTRA AND A. E. P. VELDMAN

Dept. of Mathematics, University of Groningen, The Netherlands

(Received June 25, 1971)

SUMMARY

The numerical method of solution of van de Vooren and Dijkstra [1] for the semi-infinite flat plate has been extended to the case of the parabolic cylinder. Results are presented for the skin friction, the friction drag, the pressure and the pressure drag. The drag coefficients have been checked by means of an application of the momentum theorem.

List of Symbols

a	nose radius of parabola (2.2)
A	normalization factor (3.11); part of contour D (fig. 2)
b	subscript for boundary layer quantity (3.1)
B	part of contour D (fig. 2)
C, C_1, C_2, C_3	parts of contour D (fig. 2)
$C_{Df}, \bar{C}_{Df}$	coefficients of friction and modified friction drag (8.12) and (8.14)
C_{Dp}, C_{Dp_i}	coefficients of pressure and inviscid pressure drag (8.7) and (8.9)
c_f	coefficient of local skin friction (8.10)
D	contour (fig. 2)
D_f, D_p	friction and pressure drag (8.11) and (8.6)
f, f', f'', f'''	Blasius function and derivatives (2.10). $f''(0)=0.332057336$
G	Green's function (7.3)
h	mesh size in (σ, τ)-plane (sect. 6)
i	subscript for inviscid quantity; $\sqrt{-1}$
$K, K_1, \hat{K}_1$	modified vorticity (2.11), (2.12) and (3.12) resp.
n	superscript: iteration index; subscript: differentiation in normal direction; $\boldsymbol{n}$: normal unit vector (fig. 2)
p^*, P, P_i	pressure symbols (8.1), (8.4) and (8.8) resp.
$\boldsymbol{q}$	velocity
r	radius of contour D (9.6)
R	Reynolds number (2.6)
s	curvilinear distance (8.6)
$\boldsymbol{t}$	tangential unit vector (fig. 2)
u	velocity component in x-direction
U_0	velocity at $x=-\infty$ (2.3)
v	velocity component in y-direction
w, w_1, w_1^*	complex variables (sect. 7)
x, y	Cartesian coordinates
α	numerical factor (3.11), value $\frac{1}{7}$
β	Blasius parameter, value 1.72078765
Γ	vorticity (2.4)
Δ	Laplacian
ε	small positive number (9.7)
$\eta, \eta_0, \hat{\eta}$	parabolic coordinate (2.5), (2.6) and (2.7) resp.

θ	angle between tangent to parabola and x-axis (8.6)
λ	parabolic coordinate (3.1)
$\mu, \hat{\mu}, \mu_1$	parabolic coordinate (3.1), (3.2) and (3.4) resp.
ν	kinematic viscosity
$\xi, \hat{\xi}$	parabolic coordinate (2.5) and (3.12) resp.
ρ	density
σ	transformed $\hat{\xi}$-coordinate (4.1)
τ	transformed $\hat{\eta}$-coordinate (5.2); shear stress (9.3)
φ	stream function (7.2); polar angle (9.5)
$\psi, \psi_b, \Psi, \Psi_1, \hat{\Psi}_1, \Psi_b$	stream function (2.1), (3.1), (2.5), (2.12), (3.12) and (3.4) resp.

1. Introduction

The numerical solution of the Navier–Stokes equations for laminar, incompressible flow past a semi-infinite flat plate has been obtained by van de Vooren and Dijkstra [1]. Later, the numerical method of solution has been improved by Botta and Dijkstra [2]. An important feature of both investigations is the use of parabolic coordinates which are known to be optimal for the flat plate. The natural extension of the flat plate to other body shapes is the parabolic cylinder, which is the object of the present investigation. The formulation has been chosen such that the flat plate solution arises as a special case of the procedure. The characteristic length of the parabolic cylinder is its nose radius and the Reynolds number R of the flow is based upon this length. The following three cases can be distinguished.

(i) $R=0$. This case corresponds to the flat plate and has been solved in the investigations mentioned above.

(ii) $R\to\infty$. This case corresponds to vanishing viscosity. The governing equations then are the boundary layer equations. A series expansion for the solution has been obtained by Van Dyke [3]. A numerical solution of the boundary layer equations has been presented by Smith and Clutter [4] and also, in unpublished work, by Fannelop, see Van Dyke [3].

(iii) $0< R< \infty$. The governing equations are the full Navier–Stokes equations. It is the purpose of this paper to cover this range of Reynolds numbers by solving the full equations numerically. Obviously the solution must approach the boundary layer solution if R increases without limit and this appears to be the case for the solution obtained in this investigation.

By private communication we obtained a numerical solution of the same problem by Davis [5], who solves the instationary equations and obtains the steady state solution by proceeding far enough in time. As for the space variables his method of solution agrees at several important points with the present method. By using a special boundary layer type approach during one time step followed by the treatment of the full equations in the next step, Davis' successful method produces an accurate solution in a small amount of computing time. His numerical results are compared with ours and good agreement is obtained.

By means of an application of the momentum theorem to an infinitely large circular contour we derive in sect. 9 an analytic expression for the total drag in terms of Blasius parameters. The formula which has been obtained can be seen as a generalization of Imai's result [6] for the flat plate, now extended to the case of the parabolic cylinder. The relation is used as a check for the numerical results. The deviation is within 2% for the smallest mesh size used in the present investigation when solving numerically the system of partial differential equations.

The present problem has been solved also by Dennis and Walsh [13]. Their results for the skin friction at the nose are in good agreement with those of Davis and the present results. It is believed however, that for large values of the coordinates their solution is less accurate.

2. Governing Equations and Boundary Conditions

In the two-dimensional case the Navier–Stokes equations for an incompressible viscous fluid can be combined into one equation for the stream function ψ, see e.g. Van Dyke [7],

$$\frac{\partial(\psi, \Delta\psi)}{\partial(y, x)} = \nu \Delta\Delta\psi \tag{2.1}$$

where ν is the kinematic viscosity, Δ is the Laplacian and the left-hand side denotes the Jacobian of ψ and $\Delta\psi$.

Let the infinite parabolic cylinder be given by the equation

$$y^2 = 2ax + a^2 \tag{2.2}$$

where $a > 0$ denotes the nose radius of the parabolic cylinder. The generators of the cylinder are parallel to the z-axis, so that the problem is two-dimensional. The oncoming flow is uniform and parallel to the x-axis so that we can restrict our attention to the half plane $y \geqq 0$.

If the nose radius a is set equal to 0 then the parabolic cylinder becomes the semi-infinite flat plate. The formulation of the problem has been chosen such that for $a = 0$ a correct description of the flat plate problem arises. In that case the final set of equations to be derived below becomes identical with the system obtained by van de Vooren and Dijkstra [1] in their flat plate investigation.

The boundary conditions for the two-dimensional flow past the parabola (2.2) are:

$$\left.\begin{aligned} &\psi\ (x, 0) = 0\,, \quad x < -a/2 \\ &\psi\ (x, y) = 0\,, \quad \text{at the parabola, } x \geqq -a/2 \\ &\psi_n(x, y) = 0\,, \quad \text{at the parabola, } x \geqq -a/2 \\ &\psi\ (x, y) \sim U_0 y\,, \quad x \to -\infty\,. \end{aligned}\right\} \tag{2.3}$$

Here ψ_n denotes the normal derivative of ψ at the wall and U_0 is the velocity of the oncoming flow.

The vorticity Γ is introduced by

$$\Gamma = \frac{\nu}{U_0^2}\left(\frac{\partial u}{\partial y} - \frac{\partial v}{\partial x}\right) = \frac{\nu}{U_0^2}\,\Delta\psi \tag{2.4}$$

where u and v are the velocity components.

The equations (2.1)–(2.3) express the problem in terms of dimensional, rectangular coordinates and we now introduce non-dimensional parabolic coordinates and a non-dimensional stream function in the same way as in [1], viz.

$$x + iy = \frac{\nu}{U_0}\,(\xi + i\eta)^2\,, \qquad \psi = \nu\Psi\,. \tag{2.5}$$

On parabolic coordinates the parabola (2.2) becomes

$$\eta = \eta_0 = \left(\frac{R}{2}\right)^{\frac{1}{2}} = \left(\frac{U_0 a}{2\nu}\right)^{\frac{1}{2}}, \qquad R = U_0 a/\nu \tag{2.6}$$

where R is the Reynolds number based upon the nose radius a. For $a = 0$ the Reynolds number R vanishes.

Since the flow field occupies the region $\eta > \eta_0$ in the plane of the parabolic coordinates, it is natural to introduce the coordinate $(\eta - \eta_0)$ as a measure for the distance from the wall. This modified η-coordinate is denoted by $\hat{\eta}$:

$$\hat{\eta} = \eta - \eta_0\,, \qquad \hat{\eta} \geqq 0\,. \tag{2.7}$$

Transformation of the Navier–Stokes equations (2.1) on the coordinates ξ and $\hat{\eta}$ yields

$$\left.\begin{aligned} &\Delta\Psi = 4\{\xi^2 + (\hat{\eta} + \eta_0)^2\}\,\Gamma \\ &\Delta\Gamma = \frac{\partial(\Psi, \Gamma)}{\partial(\hat{\eta}, \xi)}\,, \end{aligned}\right\} \tag{2.8}$$

where

$$\Delta = \frac{\partial^2}{\partial \xi^2} + \frac{\partial^2}{\partial \hat{\eta}^2}.$$

Use has been made of the equations (2.1), (2.4), (2.5), (2.6) and (2.7). The boundary conditions in the plane of the parabolic coordinates are:

$$\left.\begin{aligned} &\xi = 0: \quad \Psi = \Gamma = 0 \\ &\hat{\eta} = 0: \quad \Psi = \frac{\partial \Psi}{\partial \hat{\eta}} = 0 \\ &\xi \to \infty: \quad \Psi \sim \xi f(2\hat{\eta}), \ \Gamma \sim \frac{\xi}{\xi^2 + (\hat{\eta} + \eta_0)^2} f''(2\hat{\eta}) \\ &\hat{\eta} \to \infty: \quad \Psi \sim 2\xi\hat{\eta} - \beta\xi, \ \Gamma \sim 0 \text{ (exponentially)}. \end{aligned}\right\} \tag{2.9}$$

Here $f(2\hat{\eta})$ and β are Blasius quantities given by

$$\left.\begin{aligned} &2f''' + ff'' = 0, \quad f(0) = f'(0) = 0, \quad f'(\infty) = 1 \\ &f \sim 2\hat{\eta} - \beta \quad \text{for} \quad \hat{\eta} \to \infty, \quad \beta = 1.72078765 \\ &f''(0) = 0.332057336. \end{aligned}\right\} \tag{2.10}$$

The boundary condition $\Gamma = 0$ for $\xi = 0$ follows from symmetry. For a discussion of the behaviour of the solution at infinity see Veldman and Dijkstra [8].

If $a = 0$ then $\eta_0 = 0$ and the equations (2.8) with boundary conditions (2.9) then describe the flat plate problem. For the case of the flat plate Carrier and Lin [9] showed that the vorticity Γ is singular at the leading edge $\xi = \eta = \hat{\eta} = 0$. To remove the singularity the modified vorticity K has been introduced, viz.

$$K = \{\xi^2 + (\hat{\eta} + \eta_0)^2\}\Gamma. \tag{2.11}$$

This is completely in analogy with van de Vooren and Dijkstra's approach [1]. Following their method, the next step is the introduction of the departures from the Blasius solution as follows:

$$\Psi_1 = \Psi - \xi f(2\hat{\eta}), \quad K_1 = K - \xi f''(2\hat{\eta}). \tag{2.12}$$

The functions Ψ_1 and K_1 are bounded on the entire quadrant $\xi \geqq 0, \hat{\eta} \geqq 0$. The Navier–Stokes equations for Ψ_1 and K_1 become

$$\left.\begin{aligned} \Delta \Psi_1 &= 4 K_1 \\ \Delta \Omega &= \frac{\partial(\Psi_1 + \xi f, \Omega)}{\partial(\hat{\eta}, \xi)} \\ \Omega &= \frac{K_1 + \xi f''}{\xi^2 + (\hat{\eta} + \eta_0)^2} \end{aligned}\right\} \tag{2.13}$$

where instead of (2.9) the boundary conditions are now completely homogeneous, namely

$$\left.\begin{aligned} &\xi = 0: \quad \Psi_1 = K_1 = 0 \\ &\hat{\eta} = 0: \quad \Psi_1 = \frac{\partial \Psi_1}{\partial \hat{\eta}} = 0 \\ &\xi \to \infty: \quad \Psi_1 \to 0, \ K_1 \to 0 \\ &\hat{\eta} \to \infty: \quad \Psi_1 \to 0, \ K_1 \to 0 \text{ (exponentially)} \end{aligned}\right\} \tag{2.14}$$

3. Adjustment of Variables for the Case $R\to\infty$

For $R\to\infty$, i.e. $\nu\to 0$, the transformation (2.5) loses sense and should be replaced by

$$x+iy = a(\lambda+i\mu)^2\,, \quad \psi = aU_0\psi_b \tag{3.1}$$

where λ and μ are again non-dimensional parabolic coordinates and ψ_b is a non-dimensional stream function.

In analogy with (2.6) the parabolic cylinder is now given by

$$\mu = \mu_0 = \tfrac{1}{2}\sqrt{2}\,.$$

In the field we define the coordinate

$$\hat{\mu} = \mu - \tfrac{1}{2}\sqrt{2}\,. \tag{3.2}$$

In terms of the variables λ, $\hat{\mu}$ and ψ_b the Navier–Stokes equation (2.1) becomes

$$\left.\begin{aligned} &\frac{\partial(\psi_b,\omega)}{\partial(\hat{\mu},\lambda)} = \frac{1}{R}\,\Delta\omega \\ &\omega = \frac{\Delta\psi_b}{4\left\{\lambda^2+\left(\hat{\mu}+\dfrac{1}{\sqrt{2}}\right)^2\right\}} \end{aligned}\right\} \tag{3.3}$$

where

$$\Delta = \frac{\partial^2}{\partial\lambda^2}+\frac{\partial^2}{\partial\hat{\mu}^2} \quad \text{and} \quad R = U_0 a/\nu\,.$$

For the description of the boundary layer we have to introduce inner variables by putting

$$\mu_1 = R^{\frac{1}{2}}\hat{\mu}\,, \quad \Psi_b = R^{\frac{1}{2}}\psi_b\,. \tag{3.4}$$

Substitution of the transformation (3.4) into eqs. (3.3) yields in the limit $R\to\infty$ a fourth order differential equation for the stream function Ψ_b which can be integrated with respect to μ_1. The result then becomes

$$(\lambda^2+\tfrac{1}{2})\left(\frac{\partial^3\Psi_b}{\partial\mu_1^3}-\frac{\partial\Psi_b}{\partial\mu_1}\frac{\partial^2\Psi_b}{\partial\lambda\partial\mu_1}+\frac{\partial\Psi_b}{\partial\lambda}\frac{\partial^2\Psi_b}{\partial\mu_1^2}\right)+\lambda\left(\frac{\partial\Psi_b}{\partial\mu_1}\right)^2 = -2\lambda \tag{3.5}$$

where the right-hand side has been determined by matching Ψ_b for $\mu_1\to\infty$ with the outer potential flow $2\lambda\mu_1$. The boundary conditions are

$$\left.\begin{aligned} &\Psi_b(\lambda,0) = \frac{\partial\Psi_b}{\partial\mu_1}(\lambda,0) = 0 \\ &\Psi_b(0,\mu_1) = 0 \\ &\frac{\partial\Psi_b}{\partial\mu_1}(\lambda,\mu_1)\to 2\lambda \quad \text{for} \quad \mu_1\to\infty\,. \end{aligned}\right\} \tag{3.6}$$

A series expansion for the solution of (3.5) has been presented by Van Dyke [3], whereas a numerical solution has been obtained by Smith and Clutter [4]. From these investigations we infer that the solution of the boundary layer equation (3.5) is a smooth function of the coordinates λ and μ_1. This means that, for large values of $R=2\eta_0^2$, the variables λ, μ_1 and Ψ_b are the appropriate quantities for the description of the flow field. We now carry over this result to the variables used in sect. 2.

Using eqs. (2.5), (2.6), (2.7), (3.1), (3.2) and (3.4) we obtain for the relation between the two coordinate systems $(\xi,\hat{\eta})$ and (λ,μ):

$$\xi+i\hat{\eta} = \lambda R^{\frac{1}{2}}+i\mu_1\,. \tag{3.7}$$

From eqs. (2.5), (3.1) and (3.4) we infer that the relation between the stream functions is given by

$$\Psi(\xi, \hat{\eta}) \sim R^{\frac{1}{2}} \Psi_b(\lambda, \mu_1), \quad R \to \infty . \tag{3.8}$$

Application of the operator of Laplace to this result yields for large values of R:

$$K(\xi, \hat{\eta}) \sim \tfrac{1}{4} R^{\frac{1}{2}} \frac{\partial^2 \Psi_b}{\partial \mu_1^2} \tag{3.9}$$

where (2.8), (2.11) and (3.7) have been used.

Finally the result for the departures from the Blasius solution (2.12) becomes

$$\left.\begin{aligned} \Psi_1(\xi, \hat{\eta}) &\sim R^{\frac{1}{2}} \{\Psi_b(\lambda, \mu_1) - \lambda f(2\mu_1)\} \\ K_1(\xi, \hat{\eta}) &\sim R^{\frac{1}{2}} \left\{ \frac{1}{4} \frac{\partial^2 \Psi_b}{\partial \mu_1^2}(\lambda, \mu_1) - \lambda f''(2\mu_1) \right\} . \end{aligned}\right\} \tag{3.10}$$

We conclude from these expressions that normalization of the functions Ψ_1 and K_1 by means of the factor $\sqrt{R}$ will result in quantities which are $O(1)$ for $R \to \infty$. According to eq. (3.7) it is necessary to do the same with the ξ-coordinate. In order to incorporate the case $R = 0$ in the procedure the normalization factor has been set equal to

$$A = 1 + \alpha \sqrt{R} \tag{3.11}$$

with α to be determined. As a result of the considerations in sect. 4 the value $\alpha = \frac{1}{7}$ has been obtained. The variables

$$\hat{\xi} = \xi / A , \quad \hat{\eta} = \hat{\eta} , \quad \hat{\Psi}_1 = \Psi_1 / A , \quad \hat{K}_1 = K_1 / A \tag{3.12}$$

are appropriate for the entire range $0 \leqq R < \infty$ of Reynolds numbers.

Transformation of the Navier–Stokes equations (2.13) yields for $\hat{\Psi}_1$ and $\hat{K}_1$ the following equations:

$$\left.\begin{aligned} \Delta \hat{\Psi}_1 &= 4 \hat{K}_1 \\ \Delta \hat{\Omega} &= \frac{\partial(\hat{\Psi}_1 + \hat{\xi} f, \hat{\Omega})}{\partial(\hat{\eta}, \hat{\xi})} , \qquad \hat{\Omega} = \frac{\hat{K}_1 + \hat{\xi} f''}{A^2 \hat{\xi}^2 + (\hat{\eta} + \eta_0)^2} \end{aligned}\right\} \tag{3.13}$$

where

$$\Delta = \frac{1}{A^2} \frac{\partial^2}{\partial \hat{\xi}^2} + \frac{\partial^2}{\partial \hat{\eta}^2} \quad \text{and} \quad A = 1 + \tfrac{1}{7} \sqrt{R}$$

with the same boundary conditions as before, see eq. (2.14). With regard to the numerical solution of these equations there remains one difficulty and this concerns the infinite extent of the region of interest, $\hat{\xi} \geqq 0$, $\hat{\eta} \geqq 0$. This difficulty will be removed in the next sections.

4. Transformation of the Infinite $\hat{\xi}$-Region

For the semi-infinite flat plate, i.e. $R = 2\eta_0^2 = 0$, the transformation (3.12) becomes the identity. In their flat plate investigation van de Vooren and Dijkstra [1] have used the transformation

$$\sigma = 1 - \frac{\ln(1 + \hat{\xi}/2)}{\hat{\xi}/2} \tag{4.1}$$

with $\hat{\xi}$ equal to ξ, in order to map the infinite region $0 \leqq \hat{\xi} \leqq \infty$ onto the finite region $0 \leqq \sigma \leqq 1$. See fig. 1. Near $\hat{\xi} = 0$ the mapping (4.1) is regular while the behaviour for $\hat{\xi} \to \infty$ is such that it corresponds to the behaviour of the functions $\hat{\Psi}_1$ and $\hat{K}_1$. Since the arguments of van de Vooren and Dijkstra [1] also apply to the case of the parabolic cylinder the transformation (4.1) can also be used for that case. For a detailed computation of the asymptotic behaviour of $\hat{\Psi}_1$ and $\hat{K}_1$ at $\hat{\xi}$ equals infinity see Veldman and Dijkstra [8]. The factor 1/2 has been inserted in (4.1) so that the maximum value of the modified vorticity $\hat{K}_1$ at the wall is reached at $\sigma = 0.5$

and a reasonable spreading of $\hat{K}_1$ over the whole interval $0 \leqq \sigma \leqq 1$ is obtained. This is valid for $R = 0$. From the requirement that for $R = \infty$ the maximum again is reached at $\sigma = 0.5$, Veldman and Dijkstra [8] have determined the value of α, introduced in eq. (3.11), to be $\alpha = \frac{1}{7}$. It was expected that with this value of α a reasonable spreading of $\hat{K}_1$ over $0 \leqq \sigma \leqq 1$ for every Reynolds number should be obtained and this has been verified *a posteriori* from the numerical results.

5. Treatment of the $\hat{\eta}$-Coordinate

After application of the transformation (4.1) to the infinite quarter plane $\hat{\xi} \geqq 0, \hat{\eta} \geqq 0$, we obtain the strip $(0 \leqq \sigma \leqq 1, \hat{\eta} \geqq 0)$ in the $(\sigma, \hat{\eta})$-plane, see fig. 1. We now follow the approach of Botta and Dijkstra [2] for the treatment of the $\hat{\eta}$-coordinate.

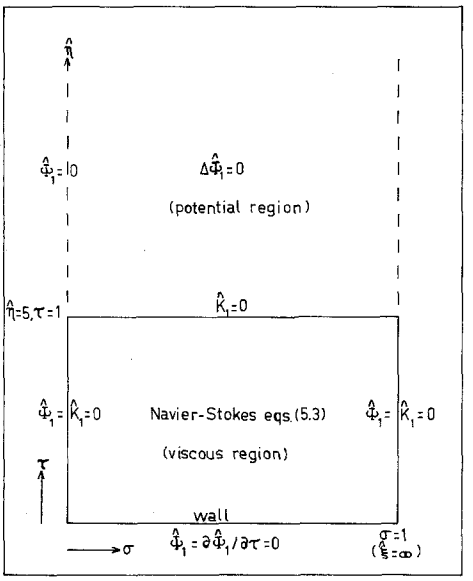

Figure 1. Configuration in the (σ, τ)-plane.

The modified vorticity $\hat{K}_1(\hat{\xi}, \hat{\eta})$ decays exponentially with $\hat{\eta} \to \infty$, see e.g. Stewartson [10] or Chang [11]. A rigorous investigation of the exponential decay of vorticity for viscous flow around a *finite* body has been given by Clark [12]. This exponential behaviour is completely in agreement with the numerical results of van de Vooren and Dijkstra [1] for the case of the flat plate. It appeared that we can safely put $\hat{K}_1 = 0$ for $\hat{\eta} \geqq 5$. In fact the numerical values of $\hat{K}_1$ for $\hat{\eta} = 5$ have the order of 10^{-7} as compared with the magnitude of unity at the wall $\hat{\eta} = 0$. It is inferred that we may take (numerically)

$$\hat{K}_1(\hat{\xi}, \hat{\eta}) = 0\,, \quad \hat{\eta} \geqq 5\,.$$

This means that the equation for the vorticity $\hat{K}_1$ in the system (3.13) can be left out of account for $\hat{\eta} \geqq 5$. The remaining equation becomes after restoring the original ξ-variable:

$$\Delta\hat{\Psi}_1 = 0\,, \quad \Delta = \frac{\partial^2}{\partial\xi^2} + \frac{\partial^2}{\partial\hat{\eta}^2}\,, \quad \hat{\eta} \geqq 5\,. \tag{5.1}$$

Thus we are led to a division of the infinite strip $(0 \leqq \sigma \leqq 1, \hat{\eta} \geqq 0)$ into two parts namely an outer potential region $(0 \leqq \sigma \leqq 1, \hat{\eta} \geqq 5)$ and an inner viscous region $(0 \leqq \sigma \leqq 1, 0 \leqq \hat{\eta} \leqq 5)$. In the potential region the equation (5.1) applies, whereas in the viscous region the full equations (3.13) must be used. For the configuration see fig. 1.

Following Botta and Dijkstra [2], the inner region where $\hat{\eta}$ runs from 0 to 5 has been normalized to the region $0 \leqq \tau \leqq 1$ so that the final form of the viscous region becomes the square $(0 \leqq \sigma \leqq 1, 0 \leqq \tau \leqq 1)$ in the (σ, τ)-plane, see fig. 1. The normalization of the coordinate $\hat{\eta}$ has

been performed first by means of the trivial transformation $\hat{\eta} = 5\tau$. However much better results have been obtained with the aid of the transformation

$$\hat{\eta} = 3\tfrac{1}{2}\tau + 1\tfrac{1}{2}\tau^4 , \quad 0 \leqq \tau \leqq 1 . \tag{5.2}$$

This transformation leads to more mesh points in the neighbourhood of the wall than when $\hat{\eta} = 5\tau$ is used. Moreover (5.2) yields a better spreading of the solution. For a detailed argument see Botta and Dijkstra [2]. Note that the singular transformation used by van de Vooren and Dijkstra [1], and later, by Davis [5] has been discarded, since the mapping (5.2) is only applied to the region $0 \leqq \hat{\eta} \leqq 5$.

For the infinite region $\hat{\eta} \geqq 5$ Botta and Dijkstra [2] have developed a special procedure, namely the Green's function approach as discussed in sect. 7. As for the viscous region $\hat{\eta} \leqq 5$ the final set of differential equations for $\hat{\Psi}_1$ and $\hat{K}_1$ has been obtained after applying the transformations (4.1) and (5.2) to (3.13) viz.

$$\left.\begin{aligned} &\Delta\hat{\Psi}_1 = 4\hat{K}_1 \\ &\Delta\hat{\Omega} = \frac{\partial(\hat{\Psi}_1 + \hat{\xi} f, \hat{\Omega})}{\partial(\tau, \sigma)} \frac{d\tau}{d\hat{\eta}} \frac{d\sigma}{d\hat{\xi}}, \quad \hat{\Omega} = \frac{\hat{K}_1 + \hat{\xi} f''}{A^2\hat{\xi}^2 + (\hat{\eta} + \eta_0)^2} \\ &\text{where} \\ &\Delta = \frac{1}{A^2}\left(\frac{d\sigma}{d\hat{\xi}}\right)^2 \frac{\partial^2}{\partial\sigma^2} + \left(\frac{d\tau}{d\hat{\eta}}\right)^2 \frac{\partial^2}{\partial\tau^2} + \frac{1}{A^2}\frac{d^2\sigma}{d\hat{\xi}^2}\frac{\partial}{\partial\sigma} + \frac{d^2\tau}{d\hat{\eta}^2}\frac{\partial}{\partial\tau}, \\ &A = 1 + \tfrac{1}{7}\sqrt{R} \quad \text{and} \quad 0 \leqq \sigma \leqq 1 , \quad 0 \leqq \tau \leqq 1 . \end{aligned}\right\} \tag{5.3}$$

For boundary conditions see fig. 1.

6. The Numerical Method of Solution

The differential equations (5.3) have been solved numerically with a finite difference method based on central differences in the (σ, τ)-plane. The square $(0 \leqq \sigma \leqq 1, 0 \leqq \tau \leqq 1)$ has been covered by a grid with netpoints

$$\sigma = ph \quad (p = 0, 1, \ldots, N)$$
$$\tau = qh \quad (q = 0, 1, \ldots, N)$$

where $Nh = 1$, h being the mesh size.

The system of difference equations has been solved by iteration whereby the new value $\hat{\Psi}_1^{(n+1)}$ is computed from the first of eqs. (5.3) and $\hat{K}_1^{(n+1)}$ from the second equation. Two complications due to boundary conditions have been encountered. The first one concerns the condition that the normal derivative $\partial\hat{\Psi}_1/\partial\tau$ should vanish at the wall $\tau = 0$. The value of the vorticity $\hat{K}_1$ at $\tau = 0$ then follows from the first equation in (5.3) which at the wall reduces to

$$\hat{K}_1 = \frac{1}{4}\left(\frac{d\tau}{d\hat{\eta}}\right)^2 \frac{\partial^2\hat{\Psi}_1}{\partial\tau^2} .$$

Taking into account that $\hat{\Psi}_1$ and $\partial\hat{\Psi}_1/\partial\tau$ must vanish for $\tau = 0$, we can take as difference equation

$$\hat{K}_1^{(n+1)}(\sigma, 0) = \frac{\hat{\Psi}_1^{(n)}(\sigma, h)}{2h^2}\left(\frac{d\tau}{d\hat{\eta}}\right)^2 + O(h) .$$

This equation was used by van de Vooren and Dijkstra [1]. However, in the present investigation the following equation is employed

$$\hat{K}_1^{(n+1)}(\sigma, 0) = \frac{8\hat{\Psi}_1^{(n)}(\sigma, h) - \hat{\Psi}_1^{(n)}(\sigma, 2h)}{8h^2}\left(\frac{d\tau}{d\hat{\eta}}\right)^2 + O(h^2) .$$

This formula is an order higher and produces more accurate results.

The second complication concerns the computation of the stream function $\hat{\Psi}_1$ along the upper side $\tau=1$ of the viscous region (see fig. 1). To overcome this difficulty we suppose that a n th approximation for $\hat{\Psi}_1$ along $\tau=1$ (or $\hat{\eta}=5$) has been obtained so far. Then the problem for $\hat{\eta}\geqq 5$ reduces to a potential problem, see eq. (5.1). The solution of this problem can be given with the aid of the Green's function for the quarter plane, as will be discussed in sect. 7. Hence we can calculate the value of $\hat{\Psi}_1^{(n)}$ along a line $\hat{\eta}=5+\Delta\hat{\eta}$, which makes it possible to find the $(n+1)$th approximation of $\hat{\Psi}_1$ along $\hat{\eta}=5$ with the difference equation for $\hat{\Psi}_1$ as it follows from the first eq. (5.3) with $\hat{K}_1=0$. Thus it is seen that the only calculations which are performed in the potential region ($\hat{\eta}\geqq 5$) are those along a line $\hat{\eta}=5+\Delta\hat{\eta}$. The boundary conditions at infinity and along the $\hat{\eta}$-axis are satisfied automatically due to the use of the Green's function (see sect. 7).

The system of difference equations has been solved by means of the successive line relaxation method. In the case of $\hat{K}_1$ the line iteration is performed with lines $\tau=$constant, since exact boundary conditions at $\sigma=0$ and $\sigma=1$ are known. The computation is started along the line $\tau=1-h$, then $\tau=1-2h$ etc., since the values of $\hat{K}_1$ along the line $\tau=1$ are prescribed, whereas the values at the wall are unknown. As for $\hat{\Psi}_1$ the line iteration has been performed using lines $\sigma=$constant, since in this case the best convergence is obtained. Because of the parabolic nature of the Navier–Stokes equations for large values of $\hat{\xi}$ ($\sigma\to 1$), the calculations for $\hat{\Psi}_1$ are started along the line $\sigma=h$.

When this method is used it appears that the convergence is 20 to 40 times as fast as in the case of the point-Jacobi iteration used in [1]. Partly this improvement is due to the fact that the relaxation factor ω can be raised from $\omega=\frac{1}{2}$ formerly until almost unity in the present work. For $\omega>1$ the iteration becomes unstable.

7. The Green's Function Approach for the Treatment of the Potential Region

In this section we present, in terms of the Green's function, the solution in the potential region. The problem may be formulated as follows (cf. fig. 1)

$$\left.\begin{aligned}
&\text{(i)}\ \ \Delta\hat{\Psi}_1^{(n)}=0\,,\ 0<\hat{\xi}<\infty\,,\ 5<\hat{\eta}<\infty\\
&\text{(ii)}\ \ \hat{\Psi}_1^{(n)}(0,\hat{\eta})=0\,,\\
&\text{(iii)}\ \ \hat{\Psi}_1^{(n)}(\hat{\xi},\hat{\eta})\ \text{is prescribed along}\ \hat{\eta}=5\,,\\
&\text{(iv)}\ \ \hat{\Psi}_1^{(n)}(\hat{\xi},\hat{\eta})\to 0\ \text{if}\ r=\sqrt{\hat{\xi}^2+\hat{\eta}^2}\to\infty\,.
\end{aligned}\right\}\tag{7.1}$$

Here $\hat{\Psi}_1^{(n)}$ is the n th-approximation to the stream function $\hat{\Psi}_1$ and Δ is the Laplacian. For simplicity we introduce the following notation

$$\hat{\Psi}_1^{(n)}(\hat{\xi},\hat{\eta})=\varphi(\lambda,\mu)\ \text{where}\ \lambda+i\mu=\hat{\xi}+i(\hat{\eta}-5)\,.\tag{7.2}$$

In terms of the new variables the solution of the Dirichlet problem (7.1) is given by

$$\varphi(P)=\int_C \varphi(Q)\,\frac{\partial}{\partial n}\,G^{(1)}(P,Q)\,ds_Q\,,\tag{7.3}$$

where $G^{(1)}$ is the Green's function of the first kind for the quarter plane $\lambda\geqq 0$, $\mu\geqq 0$ and $\partial/\partial n$ means differentiation in the outward normal direction. The point Q runs along the boundary C of the quarter plane, while $P=(\lambda,\mu)$ is an interior point. The function $G^{(1)}$ can be obtained with the aid of conformal mapping from the upper half plane (where $G^{(1)}$ is well-known) onto the quarter plane, see Botta and Dijkstra [2]. The result is

$$G^{(1)}(P,Q)=\frac{1}{2\pi}\,\mathrm{Re}\,\log\frac{w^2-w_1^2}{w^2-w_1^{*2}}\,,\quad \mathrm{Re}(w)\ \text{and}\ \mathrm{Im}(w)\geqq 0$$

where $P=(\lambda,\mu)$, $Q=(\lambda_1,\mu_1)$, $w=\lambda+i\mu$ and $w_1=\lambda_1+i\mu_1$. The star * denotes the conjugate complex quantity and Re resp. Im stands for "real part of" resp. "imaginary part of". Inserting

of the Green's function into (7.3) and using the boundary conditions (ii) and (iv) from eq. (7.1) we obtain

$$-2\pi\varphi(P) = 4\int_0^\infty \varphi(Q)\,\mathrm{Im}\,\frac{\lambda_1}{w^2-\lambda_1^2}\,d\lambda_1\,, \quad Q=(\lambda_1,0)\,. \tag{7.4}$$

This expression solves the problem (7.1) in terms of the variables (7.2). In the analysis given above it has been assumed that P is an interior point, i.e. λ, $\mu>0$. If the point P moves to the boundary $\mu=0$ then the integrand becomes singular at the point $\lambda_1=\lambda$, $\mu=0$. Numerically this means that an accurate computation of the integral (7.4) becomes difficult if the point P is close to the path of integration $\mu=0$. The difficulty is due to the fact that the function $\varphi(Q)$ is only given in discrete mesh points along $\mu=0$, i.e. $\hat{\eta}=5$. As a way out for this problem quadratic interpolation of the slowly varying function $\varphi(Q)$ has been used in order to be able to produce enough function values in the immediate neighbourhood of the (almost) singular point $\lambda_1=\lambda$. In this way a very accurate numerical procedure for integrals of the form (7.4) has been developed by Botta and Dijkstra. For the details see [2].

Using this method we obtain a better numerical approximation to the flow field at a large distance from the nose than when using van de Vooren and Dijkstra's discrete approach [1]. This is mainly due to the fact that the infinite region ξ and $\eta\to\infty$ is now better represented by means of the Green's function. In addition the (singular) η transformation used in [1] becomes superfluous (cf. sect. 5).

8. Expressions for Pressure and Skin Friction

If ρ denotes the density, $\boldsymbol{q}$ the dimensional velocity and p^* the dimensional pressure, then the Navier–Stokes equations can be written as

$$(\boldsymbol{q}\cdot\mathrm{grad})\boldsymbol{q} = -\frac{1}{\rho}\,\mathrm{grad}\,p^* - \nu\,\mathrm{rot\,rot}\,\boldsymbol{q}\,. \tag{8.1}$$

At the wall we have $\boldsymbol{q}=0$, whence (8.1) becomes

$$\mathrm{grad}\,p^* = -\rho\nu\,\mathrm{rot\,rot}\,\boldsymbol{q}\,, \qquad \hat{\eta}=0\,. \tag{8.2}$$

Combining this equation with the vorticity definition (2.4) we obtain at the wall the Cauchy–Riemann equations

$$\frac{\partial P}{\partial\xi} = \frac{\partial\Gamma}{\partial\hat{\eta}}\,, \quad \frac{\partial P}{\partial\hat{\eta}} = -\frac{\partial\Gamma}{\partial\xi}\,, \qquad \hat{\eta}=0 \tag{8.3}$$

where the non-dimensional pressure P is defined as

$$P = \frac{p^*-p_\infty^*}{\rho U_0^2}\,. \tag{8.4}$$

Using (2.11) and (2.12) we obtain for the directional derivative of the pressure along the surface of the parabola the result

$$\frac{\partial P}{\partial\xi} = \frac{1}{\xi^2+\eta_0^2}\left(\frac{\partial K_1}{\partial\hat{\eta}} - \frac{2\eta_0 K_1}{\xi^2+\eta_0^2} - \frac{2\xi\eta_0 f''(0)}{\xi^2+\eta_0^2}\right), \qquad \hat{\eta}=0\,. \tag{8.5}$$

Use has been made of the fact that $f'''(0)=0$

The pressure P can be found by integration of eq. (8.5), starting at ξ equals infinity and integrating backward along the parabola surface. The quantity K_1, being the modified vorticity, is known as a result of the computations described in sect. 6.

The pressure drag, i.e. the force in x-direction on the parabola caused by the pressure, can be written as

$$D_p = 2\rho U_0^2\int_0^s P\sin\theta\,ds' \tag{8.6}$$

where θ is the slope of the parabola and s the curvilinear distance from the top along the parabola.

The factor 2 is due to the fact that the force on the lower part of the parabola (where $y<0$) is incorporated in D_p. Using (2.5) we can write along the parabola $\eta=\eta_0$: $\sin\theta\, ds=dy=2\nu\eta_0 d\xi/U_0$, whence the non-dimensional pressure drag coefficient can be given as

$$C_{Dp}(\xi)=\frac{D_p}{\rho\nu U_0}=4\eta_0\int_0^{\xi}P\,d\xi'\,. \tag{8.7}$$

Next, we consider the behaviour of the pressure for large values of the Reynolds number R If $R=2\eta_0^2$ becomes large, then P approaches the pressure P_i which is given by inviscid theory. This potential pressure is given by

$$P_i=\frac{1}{2}\frac{\eta_0^2}{\xi^2+\eta_0^2}\quad{}^{\star} \tag{8.8}$$

For a derivation of this result see Veldman and Dijkstra [8]. The contribution to the coefficient $C_{Dp}(\infty)$ due to the inviscid pressure P_i is given by

$$C_{Dp_i}(\infty)=4\eta_0\int_0^{\infty}P_i\,d\xi'=\pi\eta_0^2\,. \tag{8.9}$$

Now, we will regard the skin friction at the parabola. When τ denotes the shear stress, the local coefficient of the skin friction is given by

$$c_f=\frac{\tau}{\frac{1}{2}\rho U_0^2}=\frac{2\nu}{U_0^2}\psi_{nn}=\frac{2}{\xi^2+\eta_0^2}K(\xi,0)\,.$$

Using eq. (2.12) we obtain

$$c_f=\frac{2\xi}{\xi^2+\eta_0^2}f''(0)+\frac{2}{\xi^2+\eta_0^2}K_1(\xi,0)\,. \tag{8.10}$$

The friction drag D_f for both sides of the parabola is given by

$$D_f=2\int_0^{s}\tau\cos\theta\,ds'\,. \tag{8.11}$$

Following the same reasoning as above for the pressure drag the non-dimensional friction drag coefficient is written in the form

$$C_{Df}=\frac{D_f}{\rho\nu U_0}=2\int_0^{\xi}\xi' c_f\,d\xi'\,. \tag{8.12}$$

With the aid of (8.10) this becomes

$$C_{Df}=4f''(0)\left\{\xi-\eta_0\arctan\left(\frac{\xi}{\eta_0}\right)\right\}+4\int_0^{\xi}\frac{\xi' K_1(\xi',0)}{\xi'^2+\eta_0^2}\,d\xi'\,. \tag{8.13}$$

The friction drag coefficient C_{Df} tends to infinity as ξ grows without limit. Therefore we introduce the modified friction drag coefficient $\bar{C}_{Df}$, by subtracting the leading term $4\xi f''(0)$. Then

$$\bar{C}_{Df}=-4f''(0)\eta_0\arctan\left(\frac{\xi}{\eta_0}\right)+4\int_0^{\xi}\frac{\xi' K_1(\xi',0)}{\xi'^2+\eta_0^2}\,d\xi'\,. \tag{8.14}$$

At $\xi=\infty$ this yields the finite result

$$\bar{C}_{Df}(\infty)=-2\pi\eta_0 f''(0)+4\int_0^{\infty}\frac{\xi' K_1(\xi',0)}{\xi'^2+\eta_0^2}\,d\xi'\,. \tag{8.15}$$

* In order that eq. (8.8) is consistent with eq. (8.5) for $R\to\infty$ we must have at the wall

$$\frac{\partial K_1}{\partial\hat{\eta}}=-\xi\frac{\eta_0^2}{\xi^2+\eta_0^2}\qquad(\hat{\eta}=0\,,\ R\to\infty)\,.$$

This formula can be obtained also by putting $\mu_1=0$ into eq. (3.5) and using eqs. (3.6), (3.7), (3.9) and (2.12).

9. Application of the Momentum Theorem

By means of an application of the momentum theorem to the flat plate, Imai [6] obtained the result

$$\bar{C}_{Df}(\infty) = \frac{\pi}{4}\beta^2 \qquad (\eta_0 = 0)\,. \tag{9.1}$$

It is the purpose of this section to generalize this result to the case of the parabolic cylinder where $\eta_0 \neq 0$.

We consider a contour D in the upper half of the (x, y)-plane. The contour consists of a circular arc C with centre at the origin, a part of the negative x-axis denoted by A and the part B which lies at the parabola surface (see fig. 2). The outward unit normal vector at the contour

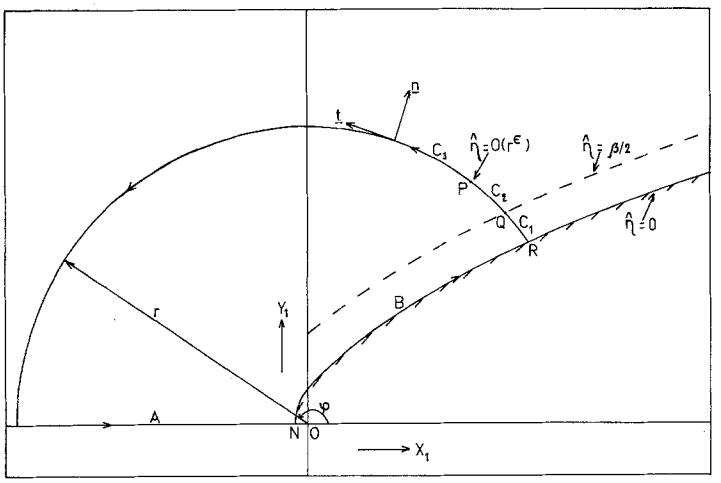

Figure 2. The contour used in the momentum theorem.

is given by $\boldsymbol{n}$ and by $\boldsymbol{t}$ we denote the tangential unit vector which corresponds with a counter clockwise rotation.

Integrating the Navier–Stokes equations (8.1) over the region σ inside the contour D, we obtain

$$\iint_\sigma \rho(\boldsymbol{q}\cdot\operatorname{grad})\boldsymbol{q}\,d\sigma = -\iint_\sigma \operatorname{grad} p^*\,d\sigma - \iint_\sigma \nu\rho \operatorname{rot}\operatorname{rot}\boldsymbol{q}\,d\sigma$$

where all quantities are dimensional. Using the fact that $\operatorname{div}\boldsymbol{q} = 0$ we obtain after an application of Gauss' theorem

$$\int_D \rho\boldsymbol{q}q_n ds = -\int_D p^*\boldsymbol{n}\,ds - \int_D \tau\boldsymbol{t}\,ds \tag{9.2}$$

where $q_n = \boldsymbol{q}\cdot\boldsymbol{n}$, s is the arc length and τ is given by

$$\tau\boldsymbol{t} = \nu\rho\boldsymbol{n}\times\operatorname{rot}\boldsymbol{q} = \rho U_0^2\Gamma\boldsymbol{t} \tag{9.3}$$

Γ denoting the vorticity (2.4).

The left-hand side of the momentum theorem (9.2) equals the outward transport of momentum per unit of time through the contour D. The right-hand side represents the pressure force plus the friction force working at the fluid inside the contour D. We are interested only in the x-component of eq. (9.2) which is written as

$$\int_C \rho u q_n ds = -\int_{B+C} \tau t_x ds - \int_{B+C} p^* n_x ds \tag{9.4}$$

where t_x and n_x are the x-components of $\boldsymbol{t}$ and $\boldsymbol{n}$. The integrations along A (see fig. 2) have been omitted since $q_n = \Gamma = n_x = 0$ along the negative x-axis. Moreover in the left-hand side the integration along B has been suppressed since the velocity $\boldsymbol{q}$ vanishes at the wall. If p^*_∞ denotes the pressure at infinity then, obviously

$$\int_{B+C} p^*_\infty n_x ds = \int_{B+C} p^*_\infty dy = 0 .$$

Combining this with (9.4) we obtain

$$\int_C \rho u q_n ds + \int_C (p^* - p^*_\infty) n_x ds + \int_C \tau t_x ds = -\int_B \tau \cos\theta ds - \int_B (p^* - p^*_\infty) \sin\theta ds \tag{9.5}$$

where θ denotes the slope of the parabola surface. With the aid of eqs. (8.4), (8.6) and (8.11) the right-hand side is seen to be equal to $-(D_f + D_p)/2$.

Next, we non-dimensionalize the coordinates by ν/U_0, the velocities by U_0, the pressure by ρU_0^2 and the drag coefficients by $\rho \nu U_0$. In the non-dimensional plane we use the parabolic coordinates (ξ, η), see eq. (2.5). In addition we introduce polar coordinates by means of

$$(\xi + i\eta)^2 = r e^{i\varphi} . \tag{9.6}$$

Using (9.3) the non-dimensional form of eq. (9.5) becomes

$$\int_C \bar{u}\bar{q}_n d\bar{s} + \int_C P \cos\varphi d\bar{s} - \int_C \Gamma \sin\varphi d\bar{s} = -\tfrac{1}{2}(C_{Df} + C_{Dp}) \tag{9.7}$$

where barred symbols are non-dimensional, P is the non-dimensional pressure (8.4) and the coefficients C_{Df} and C_{Dp} are defined in eqs. (8.12) and (8.7). It is our intention to derive an asymptotic approximation for eq. (9.7) as $r \to \infty$. To this end we divide the circular arc C in fig. 2 into three parts. The part C_1 runs from R to Q where R lies at the parabola $\hat{\eta} = 0$ and Q at the curve $\hat{\eta} = \frac{1}{2}\beta$, the latter being the displacement parabola. The part C_2 runs from Q to P where the $\hat{\eta}$-coordinate of P is supposed to be $O(r^\varepsilon)$ where ε is small but positive. The parameter ε has been introduced in order to handle the matching region where viscous flow merges into potential flow. The region $C_1 \cup C_2$ will be termed "boundary layer" and P is considered as the edge of the "boundary layer". Finally the rest of the arc C from P to the negative x-axis will be called C_3. In the "boundary layer" $C_1 \cup C_2$ we have the following estimates, using (9.6), (2.7) and (2.9)

$$\left.\begin{aligned} &\hat{\eta} = O(r^\varepsilon) \; ; \quad \varphi = O(r^{\varepsilon - \frac{1}{2}}) \; ; \quad \cos\varphi = 1 + O(r^{2\varepsilon - 1}) \\ &d\bar{s} = r d\varphi = \sqrt{r}\{1 + O(r^{2\varepsilon - 1})\} d(2\hat{\eta}) \; ; \quad \Gamma = O\left(\frac{1}{\bar{\xi}}\right) = O(r^{-\frac{1}{2}}) . \end{aligned}\right\} \tag{9.8}$$

Since the vorticity Γ is exponentially small outside the "boundary layer" we obtain using (9.8) for the contribution of the third integral in eq. (9.7) the estimate

$$\int_C \Gamma \sin\varphi d\bar{s} = \int_{C_1 \cup C_2} \Gamma \sin\varphi d\bar{s} + \exp = O(r^{2\varepsilon - \frac{1}{2}}) \tag{9.9}$$

exp denoting exponentially small terms.

Next we consider the velocity and the pressure term in (9.7). Outside the "boundary layer", i.e. along C_3, the flow is inviscid. Hence we write

$$\begin{aligned} I &\overset{\text{Def.}}{=} \int_C \bar{u}\bar{q}_n d\bar{s} + \int_C P \cos\varphi d\bar{s} = \\ &= \int_{C_3} (\bar{u}\bar{q}_n)_i d\bar{s} + \int_{C_3} P_i \cos\varphi d\bar{s} + \int_{C_1 \cup C_2} \bar{u}\bar{q}_n d\bar{s} + \int_{C_1 \cup C_2} P \cos\varphi d\bar{s} \end{aligned} \tag{9.10}$$

where the subscript i denotes the inviscid value. Through the "boundary layer" the pressure P

is known to be constant (in first order). Hence we can identify (to first order) the pressure with the pressure at the point P, which is of the order $O(r^{\varepsilon-1})$. For a detailed computation see Veldman and Dijkstra [8]. Using (9.8) we infer that the last integral in (9.10) is of the order $O(r^{2\varepsilon-\frac{1}{2}})$. Following the same argument we can write

$$\int_{C_3} P_i \cos\varphi \, d\bar{s} = \int_{C_3 \cup C_2} P_i \cos\varphi \, d\bar{s} + O(r^{2\varepsilon-\frac{1}{2}})$$

where, along C_2, the pressure P_i is defined to be the analytical continuation of the external pressure P_i. Hence the equation (9.10) becomes

$$I = \int_{C_3 \cup C_2} (\bar{u}\bar{q}_n)_i d\bar{s} + \int_{C_3 \cup C_2} P_i \cos\varphi \, d\bar{s} + \int_{C_1 \cup C_2} \bar{u}\bar{q}_n d\bar{s} - \int_{C_2} (\bar{u}\bar{q}_n)_i d\bar{s} + O(r^{2\varepsilon-\frac{1}{2}}) . \quad (9.11)$$

For the non-viscous terms in this expression we may derive pressure and velocity from the stream function (cf. (2.9))

$$\Psi = \xi(2\hat{\eta} - \beta) + O(r^{-\frac{1}{2}} \ln r) ,$$

which asymptotically corresponds to potential flow past the displacement parabola $\hat{\eta} = \beta/2$. For $r \to \infty$ the two first terms in (9.10) precisely correspond to the total inviscid drag of the displacement parabola $\hat{\eta} = \beta/2$. This drag follows from eq. (8.9) upon replacing η_0 by $\eta_0 + \beta/2$, whence

$$\lim_{r\to\infty} \left\{ \int_{C_3 \cup C_2} (\bar{u}\bar{q}_n)_i d\bar{s} + \int_{C_3 \cup C_2} P_i \cos\varphi \, d\bar{s} \right\} = -\tfrac{1}{2} C_{Dp_i}(\infty) = -\frac{\pi}{2}(\eta_0 + \tfrac{1}{2}\beta)^2 . \quad (9.12)$$

Now we evaluate the third term in eq. (9.11). In the "boundary layer" $C_1 \cup C_2$ the flow is governed for large r by the Blasius stream function $\Psi = \xi f(2\hat{\eta})$, see eq. (2.9).

The following estimate has been obtained, using (9.8),

$$\begin{aligned} \int_{C_1 \cup C_2} \bar{u}\bar{q}_n d\bar{s} &= \int_{C_1 \cup C_2} \{ f'^2(2\hat{\eta}) + O(r^{2\varepsilon-1}) \} r \, d\varphi \\ &= \sqrt{r} \int_{C_1 \cup C_2} f'^2(2\hat{\eta}) \, d(2\hat{\eta}) + O(r^{3\varepsilon-\frac{1}{2}}) \\ &= \sqrt{r} \{ 2\hat{\eta}_P - \beta - 2f''(0) \} + O(r^{3\varepsilon-\frac{1}{2}}) . \end{aligned} \quad (9.13)$$

Finally, the fourth term in (9.11) becomes

$$\begin{aligned} \int_{C_2} (\bar{u}\bar{q}_n)_i d\bar{s} &= \sqrt{r} \int_{C_2} \{ 1 + O(r^{2\varepsilon-1}) \} \, d(2\hat{\eta}) \\ &= \sqrt{r} \{ 2\hat{\eta}_P - \beta \} + O(r^{3\varepsilon-\frac{1}{2}}) \end{aligned} \quad (9.14)$$

Note that the difference between eqs. (9.14) and (9.13) is equal to the momentum thickness.

Inserting the estimates (9.9) until and including (9.14) into (9.7) yields

$$\begin{aligned} -\tfrac{1}{2}(C_{Df} + C_{Dp}) = &-\frac{\pi}{2}(\eta_0 + \tfrac{1}{2}\beta)^2 + o(1) + \sqrt{r}(2\hat{\eta}_P - \beta - 2f''(0)) + \\ &- \sqrt{r}(2\hat{\eta}_P - \beta) + O(r^{2\varepsilon-\frac{1}{2}}) + O(r^{3\varepsilon-\frac{1}{2}}) . \end{aligned}$$

If ε satisfies $0 < \varepsilon < \frac{1}{6}$ then we obtain using (9.6)

$$C_{Df} + C_{Dp} = \pi(\eta_0 + \tfrac{1}{2}\beta)^2 + 4\xi f''(0) + o(1) . \quad (9.15)$$

In terms of the modified friction drag (8.15) we obtain for $\xi = \infty$ the result

$$\bar{C}_{Df}(\infty) + C_{Dp}(\infty) = \pi(\eta_0 + \tfrac{1}{2}\beta)^2 ,$$

which agrees with Imai's result (9.1) for the flat plate $\eta_0 = 0$. Physically, this result means that the sum of pressure drag and modified friction drag is precisely equal to the (inviscid) drag of the displacement parabola $\eta = \eta_0 + \beta/2$.

10. Numerical Results

For the case of the flat plate ($R=0$) calculations have been performed for $h=\frac{1}{20}, \frac{1}{40}$ and $\frac{1}{80}$, whereas the solution for the parabola has been evaluated for $h=\frac{1}{10}, \frac{1}{20}$ and $\frac{1}{40}$. Thus it is seen that the flat plate solution has been computed to a higher accuracy than the other cases. This has been done because it concerns one single case of Reynolds number, which is of particular interest. The numerical results for the flat plate of the present investigation are the same as those obtained by van de Vooren and Dijkstra [1], though the accuracy is somewhat higher. For a detailed description of the improvements of the present numerical solution as compared with the original investigation of van de Vooren and Dijkstra we refer to Botta and Dijkstra [2]. Also in the latter report additional results for the flat plate can be found e.g. stream lines and equi-vorticity lines.

As for the present paper we confine ourselves to the results for the parabola. The flow field past the parabola has been computed for the following values of the Reynolds number $R=U_0 a/\nu$:

$$R = 10^n, \quad n = -1(1)5 .$$

These values have been chosen such that they are representative for the entire range $0 < R < \infty$.

10.1 *Local skin Friction*

The coefficient of skin friction c_f is given by eq. (8.10) in terms of the modified vorticity K_1. The results for the quantity $(\xi^2+\eta_0^2)c_f/\xi$ are presented in the limit $\xi \to 0$ in table 1 and fig. 3.

TABLE 1

Skin friction at the nose of the parabola.

$R=U_0 a/\nu$	$\lim(\xi^2+\eta_0^2)c_f/\xi$ at $\xi=0$			
	present result	Davis	Van Dyke	Dennis and Walsh
0	0.755	0.754		
0.1	0.797	0.796		
1	0.891	0.890		0.887
10	1.123	1.122		1.121
10^2	1.428	1.427	1.314	1.424
10^3	1.624	1.626	1.607	1.625
10^4	1.706	1.710	1.700	
10^5	1.734		1.730	

TABLE 2

Local skin friction $(\xi^2+\eta_0^2)c_f/\xi$ *for several Reynolds numbers R. For relation between* σ, ξ *and* $\hat{\xi}$ *see eqs.* (3.12) *and* (4.1).

σ	$\hat{\xi}$	$R=10^{-1}$	$R=1$	$R=10$	$R=10^2$	$R=10^3$	$R=10^4$	$R=10^5$
0.05	0.2142	0.799	0.891	1.122	1.427	1.623	1.704	1.733
0.15	0.7451	0.805	0.892	1.111	1.411	1.608	1.689	1.718
0.25	1.4672	0.805	0.884	1.080	1.365	1.562	1.646	1.675
0.35	2.4847	0.791	0.857	1.022	1.276	1.468	1.554	1.584
0.45	3.9872	0.766	0.815	0.940	1.145	1.316	1.398	1.428
0.55	6.3535	0.734	0.767	0.850	0.993	1.122	1.188	1.214
0.65	10.4481	0.704	0.722	0.769	0.852	0.931	0.973	0.989
0.75	18.6933	0.681	0.689	0.709	0.747	0.783	0.803	0.811
0.85	40.8656	0.668	0.671	0.676	0.687	0.698	0.704	0.706
0.95	180.5565	0.664	0.665	0.665	0.666	0.667	0.667	0.667

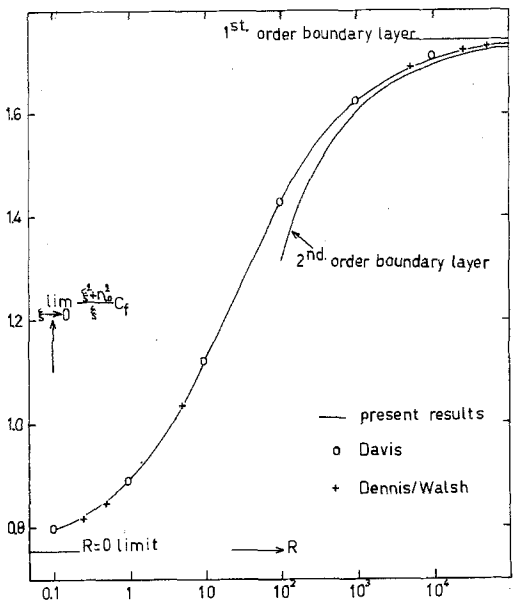

Figure 3. Skin friction at the nose.

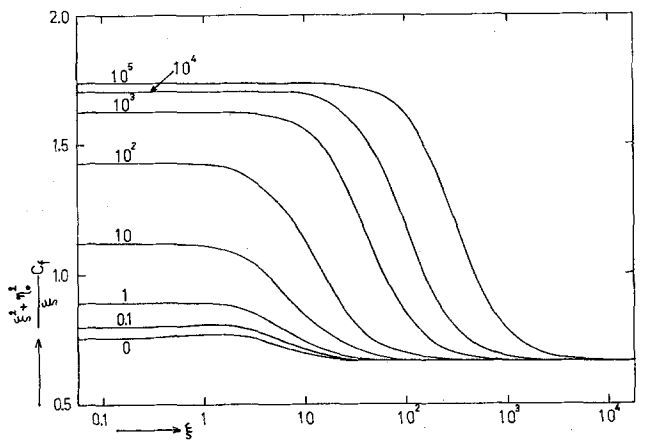

Figure 4. Skin friction at the parabola surface.

The results are compared with the values obtained by Davis [5] and those of Dennis and Walsh [13]. Also for large Reynolds number R, a comparison has been made with Van Dyke's second order boundary layer results. This analytical approximation is given by (see Van Dyke [3])

$$\lim_{\xi \to 0} \frac{\xi^2 + \eta_0^2}{\xi} c_f = 1.7432 - 4.28\, R^{-\frac{1}{2}} + O(R^{-1}) .$$

In table 2 and fig. 4 the local skin friction for $\xi > 0$ has been presented.

10.2. *Friction drag*

The friction drag $C_{Df}(\xi)$ has been defined in eq. (8.12). Since the total friction drag is the most interesting quantity, we consider, at ξ equals infinity, the modified friction drag $\bar{C}_{Df}(\infty)$ defined in eq. (8.15). The integral involved has been computed by numerical integration in the (σ, τ)-plane, viz.

$$\int_0^\infty \frac{\xi K_1(\xi, 0)}{\xi^2+\eta_0^2}\, d\xi = A \int_0^1 \frac{\hat{\xi}\hat{K}_1(\hat{\xi}, 0)}{\hat{\xi}^2+(\eta_0/A)^2}\, \frac{d\hat{\xi}}{d\sigma}\, d\sigma .$$

Use has been made of the equation (3.12). For $\hat{\xi}=\hat{\xi}(\sigma)$ see eq. (4.1). The parameter A is equal to $A=1+\sqrt{R}/7$. The integrand of the last integral can be computed from the numerical solution of eqs. (5.3). A difficulty forms the value of the integrand at $\sigma=1$ (or $\hat{\xi}=\infty$), which follows from the limiting behaviour of the modified vorticity $\hat{K}_1$ for large values of $\hat{\xi}$. For a detailed calculation see Veldman and Dijkstra [8].

TABLE 3

Modified friction drag $\bar{C}_{Df}(\infty)/(1+\sqrt{R})$.

$R=U_0 a/\nu$	Present	Davis
0.1	2.021	2.120
1	1.678	1.779
10	1.298	1.386
10^2	1.051	1.110
10^3	0.941	0.979
10^4	0.902	0.938
10^5	0.889	

The results for $\bar{C}_{Df}(\infty)$ are presented in table 3, together with the values found by Davis [5]. The values have been divided by $1+\sqrt{R}$, in order to keep them of order unity for both small and large values of R.

10.3. *Pressure and Pressure Drag*

The pressure P at the wall has been computed according to eq. (8.5) by numerical integration, using Simpson's rule. The results have been presented in table 4 and in graphical form in

TABLE 4

The pressure $P(\hat{\xi}, 0)$ *at the parabola surface for several Reynolds numbers* R.

σ	$\hat{\xi}$	$R=0.1$	$R=1$	$R=10$	$R=10^2$	$R=10^3$	$R=10^4$	$R=10^5$	$R=\infty$
0	0	1.944	0.849	0.563	0.509	0.501	0.501	0.500	0.5
0.1	0.4603	0.462	0.609	0.531	0.499	0.495	0.496	0.496	0.496
0.2	1.0771	0.178	0.317	0.428	0.459	0.471	0.475	0.477	0.477
0.3	1.9299	0.097	0.169	0.291	0.378	0.415	0.428	0.432	0.434
0.4	3.1580	0.053	0.090	0.172	0.267	0.322	0.344	0.351	0.355
0.5	5.0257	0.027	0.045	0.090	0.157	0.209	0.232	0.241	0.246
0.6	8.0939	0.012	0.020	0.040	0.076	0.109	0.126	0.132	0.136
0.7	13.7638	0.004	0.007	0.015	0.030	0.044	0.052	0.055	0.057
0.8	26.6040	0.001	0.002	0.004	0.008	0.012	0.015	0.016	0.017
0.9	72.2990	0.000	0.000	0.000	0.001	0.002	0.002	0.002	0.002

fig. 5. In table 4 we have tabulated also, the values of the inviscid pressure P_i at $R=\infty$. These numbers follow from the formula

$$P_i(\hat{\xi}, 0) = \frac{1}{2}\, \frac{1}{2(\hat{\xi}/7)^2+1}$$

which can be obtained by letting $R=2\eta_0^2$ go to infinity in equation (8.8).

The pressure drag $C_{Dp}(\infty)$ has been obtained with the aid of (8.7). Again, the numerical

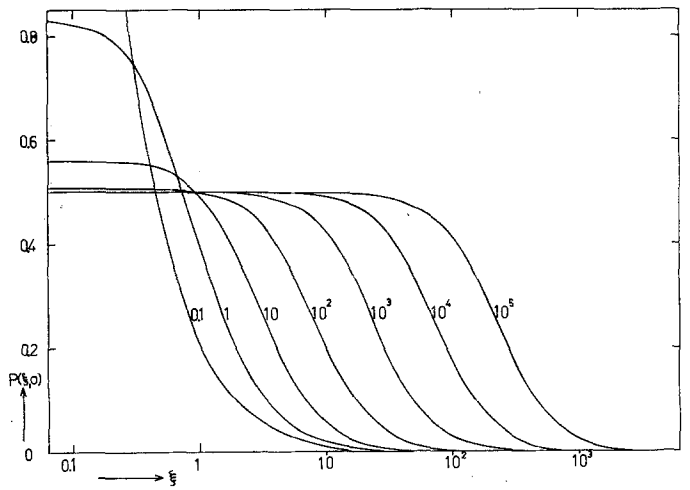

Figure 5. Pressure at the parabola surface.

TABLE 5

Pressure drag $C_{Dp}/(\sqrt{R}(1+\sqrt{R}))$.

$R = U_0 a/\nu$	Present	Davis
0.1	2.424	2.508
1	2.114	2.214
10	1.841	1.897
10^2	1.701	1.692
10^3	1.627	1.606
10^4	1.591	1.581
10^5	1.578	

integration has been performed with Simpson's rule in the σ-coordinate. The numerical values have been listed in table 5. In order to obtain finite non-zero limits at $R=0$ and $R=\infty$ we have divided the values of $C_{Dp}(\infty)$ by $\sqrt{R}(1+\sqrt{R})$. Also, in table 5, a comparison has been made with the results of Davis [5]. Note that the limiting value of the tabulated quantity for $R=\infty$ is equal to $\pi/2$, by virtue of eq. (8.9)

10.4. *Momentum Theorem*

With the aid of eq. (9.16) we can compare the numerically computed values of the modified friction drag $\bar{C}_{Df}(\infty)$ and pressure drag $C_{Dp}(\infty)$ with the exact result according to the momentum theorem. In table 6 we present the values of the left-hand side of eq. (9.16) obtained with the

TABLE 6

Check of momentum theorem (9.16)

$R = U_0 a/\nu$	$\{\pi(\eta_0+\frac{1}{2}\beta)^2\}/\{(1+\sqrt{R})^2\}$	$\{\bar{C}_{Df}(\infty)+C_{Dp}(\infty)\}/\{(1+\sqrt{R})^2\}$	
	(exact)	present	Davis
0.1	2.131	2.118	2.213
1	1.930	1.895	1.994
10	1.739	1.711	1.775
10^2	1.632	1.642	1.639
10^3	1.592	1.606	1.587
10^4	1.578	1.585	1.575
10^5	1.573	1.576	

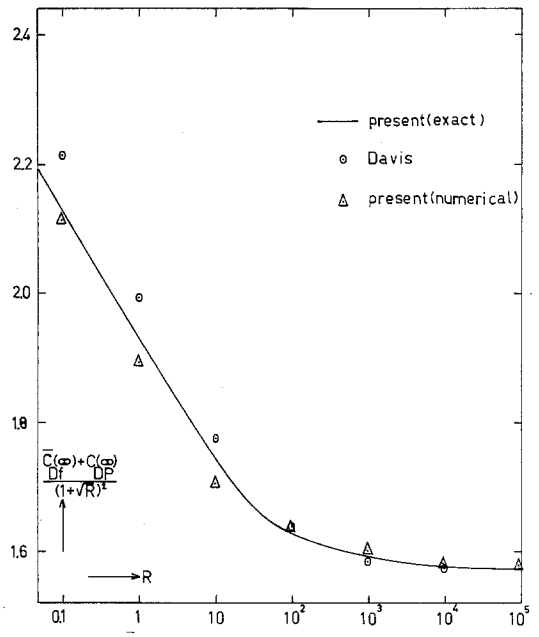

Figure 6. The total drag compared with the exact result.

present method and those found by Davis [5], as compared with the exact values of the right-hand side of eq. (9.16). The numerical values have been divided by $(1+\sqrt{R})^2$ in order to obtain results which are of order unity and which behave monotonically as a function of the Reynolds number R. The results have been plotted in fig. 6.

Acknowledgement

The authors are indebted to Prof. Dr. Ir. A. I. van de Vooren for his stimulating suggestions and advice.

REFERENCES

[1] A. I. van de Vooren and D. Dijkstra, The Navier–Stokes solution for laminar flow past a semi-infinite flat plate, *J. Eng. Math.*, 4 (1970) 9–27.
[2] E. F. F. Botta and D. Dijkstra, An improved numerical solution of the Navier–Stokes equations for laminar flow past a semi-infinite flat plate, *Report* TW-80, Dept. of Math., University of Groningen.
[3] M. D. Van Dyke, Higher approximations in boundary layer theory. Part 3. Parabola in uniform stream. *J. Fluid Mech.* 19 (1964) 145–159.
[4] A. M. O. Smith and D. W. Clutter, Solution of the incompressible laminar boundary layer equations, *Douglas Aircraft Corp. Engng. Papers* 1525 (1963).
[5] R. T. Davis, Numerical solution of the Navier–Stokes equations for laminar incompressible flow past a parabola. Submitted to the *Journal of Fluid Mechanics.*
[6] I. Imai, Second approximation to the laminar boundary layer flow over a flat plate, *J. Aeronaut. Sci.* 24 (1957) 155–156.
[7] M. D. Van Dyke, *Perturbation methods in fluid mechanics*, Academic Press, New York (1964).
[8] A. E. P. Veldman and D. Dijkstra, The numerical solution of the Navier–Stokes equations for laminar flow past a parabolic cylinder, *Report* TW-93. Dept. of Math., University of Groningen.
[9] G. F. Carrier and C. C. Lin, On the boundary layer near the leading edge of a flat plate, *Quart. Appl. Math.*, 6 (1948) 63–68.
[10] K. Stewartson, On asymptotic expansions in the theory of boundary layers. *J. Math. and Phys.*, 36 (1957) 173–191.
[11] I. D. Chang, Navier–Stokes solutions at large distances from a finite body. *J. Math. Mech.*, 10 (1961) 811–876.
[12] D. C. Clark, The vorticity at infinity for solutions of the stationary Navier–Stokes equations in exterior domains, *Mathematics J.* 20 (1971) 633–654.
[13] S. C. R. Dennis and J. D. Walsh. Numerical solutions for steady viscous flow past a parabolic cylinder in a uniform stream. Submitted to the *Journal of Fluid Mechanics.*